Research Article

Nano Research
2019, 12(9): 2330–2334

ISSN 1998-0124 CN 11-5974/O4
https://doi.org/10.1007/s12274-019-2455-z

Revealing the hidden performance of metal phthalocyanines for CO_2 reduction electrocatalysis by hybridization with carbon nanotubes

Zhan Jiang[1,2], Yang Wang[1,2] (✉), Xiao Zhang[2], Hongzhi Zheng[2], Xiaojun Wang[2], and Yongye Liang[2] (✉)

[1] *School of Materials Science and Engineering, Harbin Institute of Technology, Harbin 150001, China*
[2] *Department of Materials Science and Engineering, Southern University of Science and Technology, Shenzhen 518055, China*

Received: 8 January 2019 / **Revised:** 3 June 2019 / **Accepted:** 4 June 2019

ABSTRACT

Metal phthalocyanines (MePcs) have been considered as promising catalysts for CO_2 reduction electrocatalysis due to high turnover frequency and structural tunability. However, their performance is often limited by low current density and the performance of some systems is controversial. Here, we report a carbon nanotube (CNT) hybridization approach to study the electrocatalytic performance of MePcs (Me = Co, Fe and Mn). MePc molecules are anchored on CNTs to form the hybrid materials without noticeable molecular aggregations. The MePc/CNT hybrids show higher activities and better stabilities than their molecular counterparts. FePc/CNT is slightly less active than CoPc/CNT, but it could deliver higher Faradaic efficiencies for CO production at low overpotentials. In contrast, the catalytic performance of MePc molecules directly loaded on substrate is hindered by molecular aggregation, especially for FePc and MnPc. Our results suggest that carbon nanotube hybridization is an efficient approach to construct advanced MePc electrocatalysts and to understand their catalytic performance.

KEYWORDS

CO_2 reduction, electrocatalysis, carbon nanotube, metal phthalocyanine, hybrid

1 Introduction

Electrocatalytic reduction of CO_2 is a promising avenue to convert CO_2 into valuable chemicals [1–4]. Currently, it suffers from high overpotential of the operation and low selectivity of the desired products [5–8]. Development of high-performance catalysts is of great importance for the employment of this technology [9, 10]. Since the early studies by Meshitsuka et al. and Lewis et al. [11, 12], metal phthalocyanines (MePcs) have been considered as an interesting class of electrocatalysts for CO_2 reduction [13–17]. These molecules are easily accessible and can deliver good turnover frequency (TOF) and high product selectivity [18, 19]. Further, their structures are well-defined for structure–property relationship understanding and can be tuned in either the metal center or phthalocyanine ring to improve the catalytic performance [20–22].

Most reported MePc systems generally operate at low loading and exhibit low reduction current densities compared to metal counterparts [23–26]. Further, despite well-defined structures, the catalytic performance of MePcs reported in literature could vary significantly. For example, cobalt(II) phthalocyanine (CoPc) is a well-studied phthalocyanine molecule and has been identified as the most active catalyst to convert CO_2 into CO among the phthalocyanine systems, but the reported Faradaic efficiencies (FEs) of CO (FE(CO)s) range from 37% to 98% under similar reaction conditions in Refs. [19, 27]. In another case, iron(II) phthalocyanine (FePc) was reported to be an active electrocatalyst with high FE(CO)s by Furuya et al. [28]. However, a recent study showed that it exhibited low activities and low FE(CO)s [27]. These problems are mainly originated from the molecular structure of MePc: They are semiconducting and have strong intermolecular interactions due to the large π system [29, 30]. As a result, when they are loaded on electrode by drop-drying or dip-coating, molecular aggregates are easily formed [31]. Recently, we developed a hybridization approach to improve the catalytic performance of CoPc by anchoring CoPc molecules on side walls of carbon nanotubes (CNTs) [31]. The CoPc/CNT hybrid exhibits significantly higher catalytic activity and CO selectivity than CoPc loaded on the electrode by drop-drying, and is able to deliver high current density and high TOF simultaneously. It is found that the hybridization can prevent the aggregation of CoPc molecules and enable the favorable charge transport from electrode to the active sites.

Herein, we employ the CNT hybridization approach to study a series of metal phthalocyanines for CO_2 electroreduction. MePc/CNT (Me = Co, Mn, Fe) hybrids are synthesized with MePc molecules anchoring on CNTs with no observed molecular aggregation. CoPc/CNT is the most active with high CO production current. In terms of product selectivity, FePc/CNT exhibits higher FE(CO)s of over 98% at low overpotentials. However, FePc/CNT suffers from low catalytic stability at high overpotentials. All the hybrids show higher activities and better stabilities than their molecular counterparts directly loaded on electrode. Among the neat molecules, only CoPc shows appreciable activities for CO_2 electroreduction.

2 Experimental

2.1 Chemicals

Manganese(II) phthalocyanine (MnPc), CoPc, FePc, N,N-dimethylformamide (DMF) and high-purity titanium (Ti) foil were purchased from commercial suppliers, and used without further purification. CNTs were purchased from C-Nano (FT 9100). Carbon fiber paper (CFP, TGP-H-060) was purchased from Fuel Cell Store.

Address correspondence to Yongye Liang. liangyy@sustech.edu.cn; Yang Wang, wangy33@mail.sustech.edu.cn

CNTs were purified by calcining at 500 °C and washing with HCl (5 M) solution as reported in Ref. [31]. $KHCO_3$ aqueous solution was purified by electrolysis in a two-electrode setup using a pair of 10 × 5 cm^2 Ti foil electrodes. The electrolysis was performed at 150 μA for at least 24 h.

2.2 Preparation of the hybrid materials

The MePc/CNT hybrids were prepared by a DMF sonication approach reported in Ref. [31]. Generally, purified CNTs (30 mg) were dispersed in 20 mL DMF by sonication. Then, MePc (~ 1.5 mg) in 10 mL DMF was added into the CNT suspension. The mixture was sonicated for 30 min and then stirred at room temperature (RT) for overnight. The solid was collected and washed with DMF, ethanol and water successively. Finally, the MePc/CNT precipitate was dried in vacuo to yield the final product.

2.3 Material characterizations

Transmission electron microscopy (TEM) measurements were performed on a FEI Tecnai G2 F30 transmission electron microscope. Scanning electron microscopy (SEM) and energy dispersive X-ray spectroscopy (EDS) were conducted on a TESCAN MIRA3 LM microscope. Inductively coupled plasma mass spectrometry (ICP-MS) was performed on an Agilent Technologies 7700 series instrument.

2.4 Electrochemical measurements

All electrochemical measurements were conducted by a CHI 660E Potentiostat with a three-electrode configuration. Generally, the hybrid catalyst ink was prepared by dispersing 2.0 mg sample in 1 mL Nafion solution (0.0325 wt.% in ethanol) with sonication for 1 h. The MePc ink was prepared in DMF (2.0 mg/mL). The working electrode was prepared by drop-drying 100 μL catalyst ink onto a 0.50 cm^2 CFP (loading: 0.40 mg/cm^2). A KCl saturated Ag/AgCl electrode and a graphite rod were used as the reference and counter electrodes, respectively, in an anion exchange membrane separated H-cell. Unless otherwise stated, the electrolyte was a CO_2-saturated 0.10 M $KHCO_3$ solution (pH 6.8, pre-purified). All potentials were converted to versus reversible hydrogen electrode (RHE) with *iR* corrections. The flow rate of CO_2 (99.999%) was 5 mL/min. The cyclic voltammetry (CV) was performed in 0.10 M phosphate buffer solution (PBS) under argon (pH 6.8). Gas product analyses were conducted by a gas chromatograph (GC, SRI 8610C) as reported in Ref. [31]. The TOF_{CO} is calculated using the equation below

$$TOF_{CO} = \frac{J_{co}}{ne\mu N_A}$$

where J_{CO} is the partial current for CO formation; n = 2, indicating two electrons needed to reduce one CO_2 molecule to CO; e is the electron charge (e = 1.602 × 10^{-19} C); μ is the mole number of MePc molecules on electrodes; and N_A is the Avogadro's number (N_A = 6.02 × 10^{23} mol^{-1}).

3 Results and discussion

The MePc/CNT hybrids were synthesized by interacting the MePc molecules and CNTs in DMF solution. The metal content in the hybrid can be tuned by varying the input ratio of MePc to CNT, and is finally determined by ICP-MS. In this study, the metal content was controlled to be around 0.30 wt.% in all the hybrids for fairly comparing their electrocatalytic activities (Table S1 in the Electronic Supplementary Material (ESM)).

Figure 1(a) shows the SEM image of the FePc/CNT hybrid loaded on the CFP substrate. The CFP substrate is covered by the fluffy CNT stacks. The EDS spectrum on such stacks reveals the existence of N and Fe signals, suggesting the distribution of FePc molecules on CNTs. We further used TEM to investigate the fine morphology of the hybrid. As shown in Fig. 1(b), nanotubular structures are observed, indicating that FePc molecules are anchored on the side walls of CNTs and there is no noticeable aggregation of FePc molecules. The CoPc/CNT and MnPc/CNT hybrids show similar morphology as FePc/CNT (Figs. S1 and S2 in the ESM).

In contrast to the hybrids, MePc molecules directly loaded on the CFP substrate show significant aggregation. As shown in Fig. 1(c), some of the carbon fibers are covered by the FePc molecules as confirmed by the EDS mapping. The surface is rough and aggregates with size of around 1 μm are observed. There are also some microcrystals of the FePc molecules on CFP (Fig. 1(d)). Similar microcrystals with larger size are observed in the CoPc and MnPc samples, possibly due to the lower solubility of CoPc and MnPc than FePc (Figs. S1(d) and S2(d) in the ESM).

To characterize the electrocatalytic performance of CO_2 reduction, the catalysts were deposited on CFP and measured in CO_2-saturated 0.10 M $KHCO_3$ (pH 6.8). The MePc electrodes are prepared by drop-drying of DMF solutions on CFP as DMF is a better solvent for MePc than ethanol [31]. The mass loading of the catalysts is 0.40 mg/cm^2, which corresponds to the molecular loading (MePc) of ~ 2.1 × 10^{-8} mol/cm^2 for MePc/CNT and ~ 7.0 × 10^{-7} mol/cm^2 for MePc. During the linear sweep voltammetry (LSV) measurements, both CoPc/CNT and FePc/CNT show significant cathodic current below −0.40 V, while MnPc/CNT exhibits slightly larger current density than the blank substrate below −0.70 V (Fig. 2(a)). CoPc/CNT is the most active with the largest reduction current densities and FePc/CNT is slightly less active. Although neat MePcs directly loaded on CFP have ~ 33 times larger molecular loading than the MePc/CNT hybrids, they give substantially smaller reduction current densities (Fig. 2(b)). As revealed by the morphology studies, CNT hybridization could prevent the aggregation of MePc molecules and benefit the exposure of active sites, which may explain such activity differences. CoPc is still the most active one among the MePcs, and it can deliver a reduction current density of −10 mA/cm^2 at −0.79 V, which is 0.18 V more negative than CoPc/CNT. Unlike their hybrid counterparts, the reduction current density of FePc is much smaller than that of CoPc.

Controlled current density electrolysis measurements were further conducted and the reduction products were quantitatively analyzed (gas products by online GC). Figures 3(a) and 3(b) show the chronopotentiometry of the CoPc/CNT hybrid and neat CoPc, respectively. The CoPc/CNT hybrid exhibits a current density of −0.50 mA/cm^2 at −0.40 V and a high current density of −12 mA/cm^2 at −0.64 V. Neat CoPc shows inferior performance, the initial potential

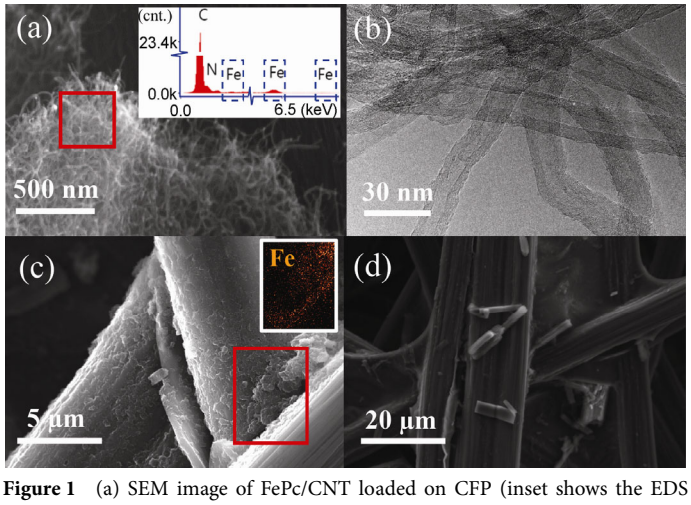

Figure 1 (a) SEM image of FePc/CNT loaded on CFP (inset shows the EDS spectrum of the outlined area). (b) TEM image of FePc/CNT. (c) SEM image of FePc loaded on CFP (inset shows the EDS mapping of Fe element in the outlined area). (d) SEM image of FePc microcrystals on CFP.

for a current density of −0.50 mA/cm² is −0.51 V. Further, the operation stability of the CoPc/CNT hybrid is better than neat CoPc. Little overpotential increase (< 5 mV) is observed in the CoPc/CNT hybrid after 40 mins operation at each current density (Fig. 2(a)). However, significant overpotential increase is observed in CoPc during the measurements at −0.25 mA/cm² and −0.50 mA/cm² (Fig. 2(b)). The potential changes from −0.51 to −0.53 V during 40 min at current density of −0.50 mA/cm². CO and H_2 are the major reduction products, and the determined FE(CO)s and FE(H_2)s are shown in Fig. 2(c) and Fig. S3 in the ESM, respectively. The CoPc/CNT hybrid could deliver a high FE(CO) of over 90% at potential below −0.60 V. Interestingly, neat CoPc delivers even higher FE(CO)s than CoPc/CNT, especially at low overpotentials. For example, the FE(CO) of CoPc is around 85% at −0.45 V, while it is 64% for CoPc/CNT. The CV measurements may explain such unexpected result (Fig. 3(d)). The reduction peak at around −0.39 V is assigned to the reduction of Co(II) to Co(I), which is considered as the active site for CO_2 reduction [32]. The reduction peak of CoPc locates at a more positive potential than that of CoPc/CNT, suggesting the molecular aggregations in CoPc sample may benefit the formation of Co(I) at low overpotentials, which can account for its better selectivity to CO. By comparing the area of redox peaks, it is clear that CoPc/CNT has larger number of electro-active sites than neat CoPc, though the molecular loading of CoPc/CNT is only ~ 1/35 of neat CoPc. As a result, the partial current densities for CO production of the CoPc/CNT hybrid are multiple times higher than those of neat CoPc at various potentials (Fig. S4 in the ESM). A long-term chronopotentiometry measurement was conducted at −12 mA/cm² for 15 h, CoPc/CNT exhibits little decay on potential and product selectivity during the operation (Fig. S10(a) in the ESM), indicating its good stability.

FePc/CNT and MnPc/CNT are less active than CoPc/CNT (Figs. 4(a) and 5(a)). To deliver a reduction current density of −1.0 mA/cm², CoPc/CNT, FePc/CNT and MnPc/CNT require a potential of −0.44, −0.47 and −0.91 V, respectively. Interestingly, FePc/CNT is superior to CoPc/CNT with higher FE(CO)s at low overpotentials. The FE(CO)s of FePc/CNT from −0.44 to −0.52 V are over 98%, while they are below 80% for CoPc/CNT. However, FePc/CNT has catalytic stability problem, especially at high overpotentials. For example, the potential changes from −0.58 to −0.78 V after 40 min operation at current density of −4.0 mA/cm². Significant potential increase is also observed in the chronopotentiometry measurement at −1.0 mA/cm² for 10 h (Fig. S10(b) in the ESM). Previous theoretical calculations suggested that iron active site has strong binding with CO, which may explain such instability [27, 33]. Different from CoPc/CNT and FePc/CNT, MnPc/CNT exhibits lower selectivity for CO_2 reduction than hydrogen evolution (Fig. 5(c), and Figs. S5 and S6 in the ESM). As shown in the CV curves in Fig. 5(d), MnPc/CNT is more difficult to be reduced compared to CoPc/CNT and FePc/CNT, which may explain its low catalytic activities. It should be noted that the catalytic performance of MnPc/CNT is still much better than the MnPc catalyst reported previously with FE(CO) < 7% [15].

Both neat FePc and MnPc exhibit lower activities compared to their hybrid counterparts, especially for FePc (Figs. 4(b) and 5(b)). For example, to deliver a reduction current density of −0.5 mA/cm², FePc requires a potential of −0.78 V (initial), which is around 0.30 V more negative than FePc/CNT (Fig. 4(b)). The FE(CO)s of FePc are much lower than those of FePc/CNT (Fig. 4(c)). Actually, neat FePc

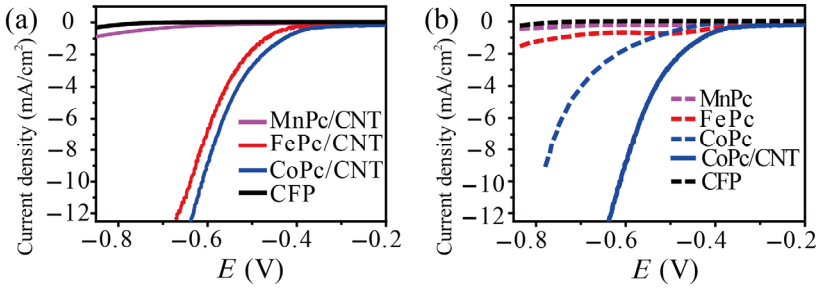

Figure 2 Linear sweep voltammetry curves of (a) MePc/CNT and (b) MePc directly loaded on CFP. The tests were conducted in CO_2-saturated 0.10 M $KHCO_3$ electrolyte with a scan rate of 5 mV/s.

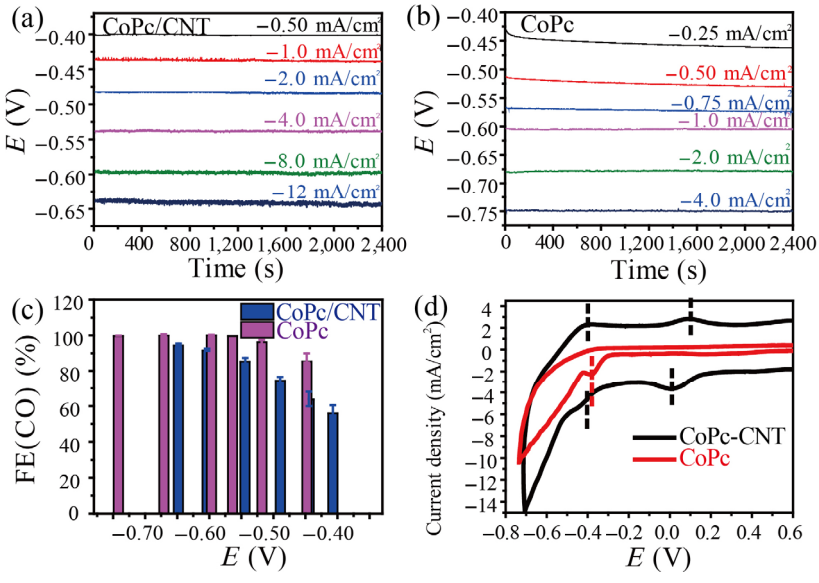

Figure 3 Chronopotentiometry of (a) CoPc/CNT and (b) neat CoPc in CO_2-saturated 0.10 M $KHCO_3$. (c) Faradaic efficiencies of CO formation at different potentials for CoPc/CNT and CoPc based on the chronopotentiometry measurements. (d) Cyclic voltammetry curves of CoPc/CNT (black line) and CoPc (red line) in argon saturated 0.10 M PBS with a san rate of 0.40 V/s.

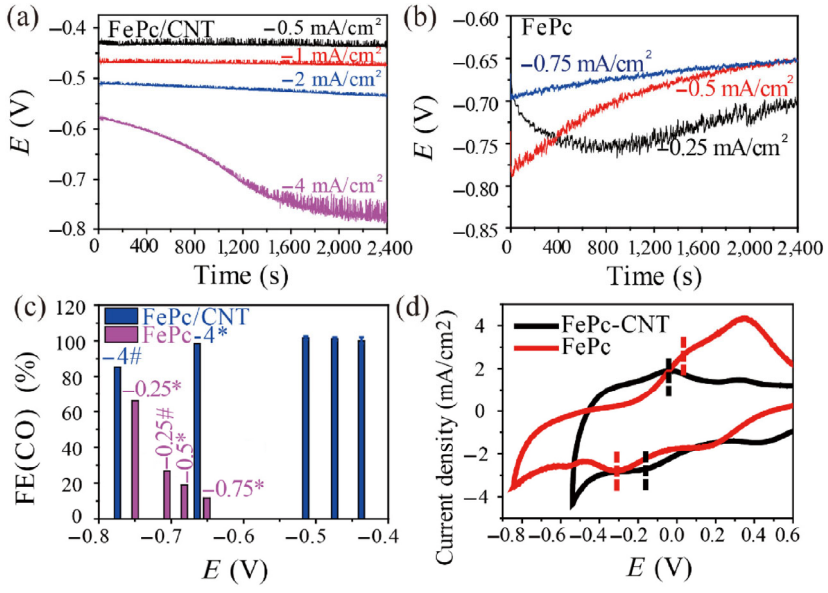

Figure 4 Chronopotentiometry of (a) FePc/CNT and (b) neat FePc in CO_2-saturated 0.10 M $KHCO_3$. (c) Faradaic efficiencies of CO formation at different potentials for FePc/CNT and FePc based on the chronopotentiometry measurements (the current density is shown in the unstable runs, and * was taken after 20 min, while # was taken after 40 min). (d) Cyclic voltammetry curves of FePc/CNT (black line) and FePc (red line) in argon saturated 0.10 M PBS with a san rate of 0.40 V/s.

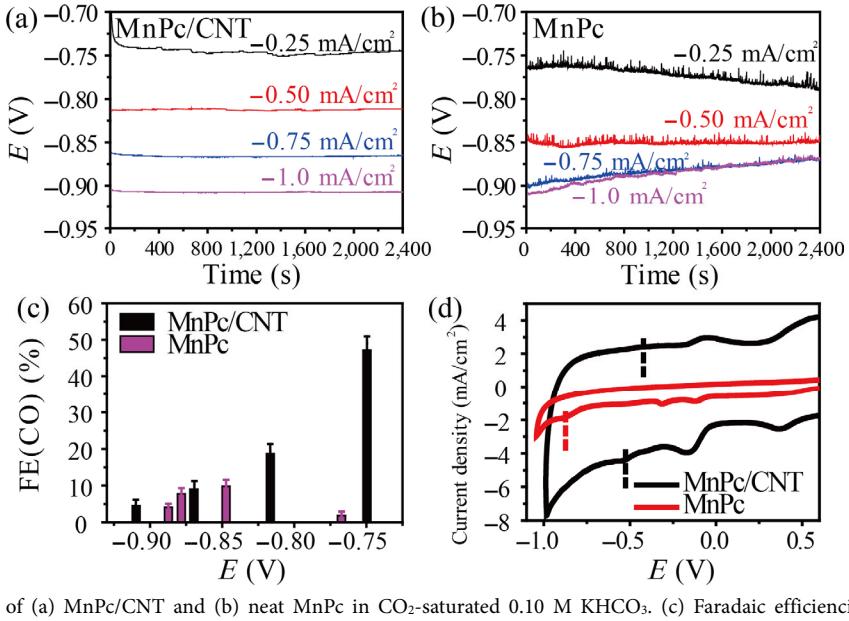

Figure 5 Chronopotentiometry of (a) MnPc/CNT and (b) neat MnPc in CO_2-saturated 0.10 M $KHCO_3$. (c) Faradaic efficiencies of CO formation at different potentials for MnPc/CNT and MnPc based on the chronopotentiometry measurements. (d) Cyclic voltammetry curves of MnPc/CNT (black line) and MnPc (red line) in argon saturated 0.10 M PBS with a san rate of 0.40 V/s.

and MnPc exhibit abnormal behaviors, and their potentials become more positive with time at larger current densities during the chronopotentiometry measurements. The determined FE(CO)s decrease with time for FePc (Fig. 4(c) and Fig. S7 in the ESM). It suggests that the catalytic performance may be dominated by the decayed products, which favor hydrogen evolution reaction (HER). In CV, FePc exhibits similar currents compared to FePc/CNT, possibly due to the better dispersity of FePc. However, the redox peaks of FePc locate at more negative potentials than FePc/CNT, and a new pair of redox peaks are observed in FePc. As shown in Fig. 5(d), the CV current of MnPc is smaller than MnPc/CNT due to the strong aggregation of MnPc (Fig. S2 in the ESM). The redox peaks of MnPc also locate at more negative potentials compared to those of MnPc/CNT. Similar to CoPc/CNT, the partial current densities for CO production of the FePc/CNT and MnPc/CNT hybrids are substantially higher than those of their molecular counterparts (Figs. S8 and S9 in the ESM).

We further investigated the TOFs of CoPc and FePc at a variety of loadings and compared with CoPc/CNT and FePc/CNT (Fig. S11 in the ESM). Because it is not readily to determine the number of electrochemically active molecules from the broad CV peaks, the TOF values are calculated by counting all the molecules loaded on electrodes. The actual TOFs are higher than the calculated TOF values. As the loading reduces, the calculated TOF increases due to less molecular aggregation and improved catalyst utilization. When the CoPc loading is below ~ 2×10^{-10} mol/cm^2, the TOF_{CO} values remain similar, suggesting that molecular aggregation is less significant and the activities are close to the intrinsic ones. At −0.61 V, the TOF_{CO} of CoPc with the loading of 4.5×10^{-11} mol/cm^2 is calculated to be 1.5 s^{-1}, which is similar to the one of CoPc/CNT (2.2 s^{-1}) (Fig. S11(a) in the ESM). Similarly, the TOF_{CO} of FePc with the loading of 9.9×10^{-11} mol/cm^2 is calculated to be 0.62 s^{-1} at −0.66 V, which is close to the one of FePc/CNT (0.90 s^{-1}) (Fig. S11(b) in the ESM). These results indicate that CNT hybridization is helpful to reveal the intrinsic

activities of MePc molecules and deliver higher current densities.

4 Conclusions

In summary, we prepare a series of metal (Co, Fe, Mn) phthalocyanine/carbon nanotube hybrids and study their catalytic performance for CO_2 electroreduction. Both CoPc/CNT and FePc/CNT are active catalysts to reduce CO_2 to CO and are able to deliver a reduction current density of −1.0 mA/cm^2 above −0.47 V. FePc/CNT is just slightly less active than CoPc/CNT, but superior to CoPc/CNT with higher FE(CO)s at low overpotentials. For metal phthalocyanine molecules directly loaded on electrode, their catalytic performance could be blocked by the molecular aggregations. Thus, the MePc/CNT hybrids generally exhibit improved catalytic performance (such as reduction current density, stability, and selectivity) compared to their molecular counterparts. Our studies suggest that carbon nanotube hybridization is an efficient approach to construct advanced molecular electrocatalysts for CO_2 electrocatalysis. Further, the hybridization also provides a feasible platform to understand the intrinsic properties of MePcs for electrocatalysis.

Acknowledgements

Y. Y. L. acknowledges financial supports from Shenzhen fundamental research funding (No. JCYJ20160608140827794).

Electronic Supplementary Material: Supplementary material (Figs. S1–S11 and Table S1) is available in the online version of this article at https://doi.org/10.1007/s12274-019-2455-z.

References

[1] Sakakura, T.; Choi, J. C.; Yasuda, H. Transformation of carbon dioxide. *Chem. Rev.* **2007**, *107*, 2365–2387.

[2] Qiao, J. L.; Liu, Y. Y.; Hong, F.; Zhang, J. J. A review of catalysts for the electroreduction of carbon dioxide to produce low-carbon fuels. *Chem. Soc. Rev.* **2014**, *43*, 631–675.

[3] Nielsen, D. U.; Hu, X. M.; Daasbjerg, K.; Skrydstrup, T. Chemically and electrochemically catalysed conversion of CO_2 to CO with follow-up utilization to value-added chemicals. *Nat. Catal.* **2018**, *1*, 244–254.

[4] Seh, Z. W.; Kibsgaard, J.; Dickens, C. F.; Chorkendorff, I.; Nørskov, J. K.; Jaramillo, T. F. Combining theory and experiment in electrocatalysis: Insights into materials design. *Science* **2017**, *355*, eaad4998.

[5] Weekes, D. M.; Salvatore, D. A.; Reyes, A.; Huang, A.; Berlinguette, C. P. Electrolytic CO_2 reduction in a flow cell. *Acc. Chem. Res.* **2018**, *51*, 910–918.

[6] Varela, A. S.; Ju, W.; Strasser, P. Molecular nitrogen-carbon catalysts, solid metal organic framework catalysts, and solid metal/nitrogen-doped carbon (MNC) catalysts for the electrochemical CO_2 reduction. *Adv. Energy Mater.* **2018**, *8*, 1703614.

[7] Diercks, C. S.; Liu, Y. Z.; Cordova, K. E.; Yaghi, O. M. The role of reticular chemistry in the design of CO_2 reduction catalysts. *Nat. Mater.* **2018**, *17*, 301–307.

[8] Lin, S.; Diercks, C. S.; Zhang, Y. B.; Kornienko, N.; Nichols, E. M.; Zhao, Y. B.; Paris, A. R.; Kim, D.; Yang, P. D.; Yaghi, O. M. et al. Covalent organic frameworks comprising cobalt porphyrins for catalytic CO_2 reduction in water. *Science* **2015**, *349*, 1208–1213.

[9] Lu, Q.; Jiao, F. Electrochemical CO_2 reduction: Electrocatalyst, reaction mechanism, and process engineering. *Nano Energy* **2016**, *29*, 439–456.

[10] Kumar, B.; Brian, J. P.; Atla, V.; Kumari, S.; Bertram, K. A.; White, R. T.; Spurgeon, J. M. New trends in the development of heterogeneous catalysts for electrochemical CO_2 reduction. *Catal. Today* **2016**, *270*, 19–30.

[11] Meshitsuka, S.; Ichikawa, M.; Tamaru, K. Electrocatalysis by metal phthalocyanines in the reduction of carbon dioxide. *J. Chem. Soc. Chem. Commun.* **1974**, 158–159.

[12] Lieber, C. M.; Lewis, N. S. Catalytic reduction of carbon dioxide at carbon electrodes modified with cobalt phthalocyanine. *J. Am. Chem. Soc.* **1984**, *106*, 5033–5034.

[13] Manbeck, G. F.; Fujita, E. A review of iron and cobalt porphyrins, phthalocyanines and related complexes for electrochemical and photochemical reduction of carbon dioxide. *J. Porphyr. Phthalocya.* **2015**, *19*, 45–64.

[14] Han, N.; Wang, Y.; Ma, L.; Wen, J. G.; Li, J.; Zheng, H. C.; Nie, K. Q.; Wang, X. X.; Zhao, F. P.; Li, Y. F. et al. Supported cobalt polyphthalocyanine for high-performance electrocatalytic CO_2 reduction. *Chem* **2017**, *3*, 652–664.

[15] Furuya, N.; Koide, S. Electroreduction of carbon dioxide by metal phthalocyanines. *Electrochim. Acta* **1991**, *36*, 1309–1313.

[16] Abe, T.; Yoshida, T.; Tokita, S.; Taguchi, F.; Imaya, H.; Kaneko, M. Factors affecting selective electrocatalytic CO_2 reduction with cobalt phthalocyanine incorporated in a polyvinylpyridine membrane coated on a graphite electrode. *J. Electroanal. Chem.* **1996**, *412*, 125–132.

[17] Kramer, W. W.; McCrory, C. C. L. Polymer coordination promotes selective CO_2 reduction by cobalt phthalocyanine. *Chem. Sci.* **2016**, *7*, 2506–2515.

[18] Zhu, M. H.; Ye, R. Q.; Jin, K.; Lazouski, N.; Manthiram, K. Elucidating the reactivity and mechanism of CO_2 electroreduction at highly dispersed cobalt phthalocyanine. *ACS Energy Lett.* **2018**, *3*, 1381–1386.

[19] Morlanés, N.; Takanabe, K.; Rodionov, V. Simultaneous reduction of CO_2 and splitting of H_2O by a single immobilized cobalt phthalocyanine electrocatalyst. *ACS Catal.* **2016**, *6*, 3092–3095.

[20] Pan, Y.; Lin, R.; Chen, Y. J.; Liu, S. J.; Zhu, W.; Cao, X.; Chen, W. X.; Wu, K. L.; Cheong, W. C.; Wang, Y. et al. Design of single-atom Co-N_5 catalytic site: A robust electrocatalyst for CO_2 reduction with nearly 100% CO selectivity and remarkable stability. *J. Am. Chem. Soc.* **2018**, *140*, 4218–4221.

[21] Yang, H. B.; Hung, S. F.; Liu, S.; Yuan, K. D.; Miao, S.; Zhang, L. P.; Huang, X.; Wang, H. Y.; Cai, W. Z.; Chen, R. et al. Atomically dispersed Ni(I) as the active site for electrochemical CO_2 reduction. *Nat. Energy* **2018**, *3*, 140–147.

[22] Abe, T.; Imaya, H.; Yoshida, T.; Tokita, S.; Schlettwein, D.; Wöhrle, D.; Kaneko, M. Electrochemical CO_2 reduction catalysed by cobalt octacyanophthalocyanine and its mechanism. *J. Porphyr. Phthalocya.* **1997**, *1*, 315–321.

[23] Weng, Z.; Wu, Y. S.; Wang, M. Y.; Jiang, J. B.; Yang, K.; Huo, S. J.; Wang, X. F.; Ma, Q.; Brudvig, G. W.; Batista, V. S. et al. Active sites of copper-complex catalytic materials for electrochemical carbon dioxide reduction. *Nat. Commun.* **2018**, *9*, 415.

[24] Dinh, C. T.; Burdyny, T.; Kibria, G.; Seifitokaldani, A.; Gabardo, C. M.; de Arquer, F. P. G.; Kiani, A.; Edwards, J. P.; De Luna, P.; Bushuyev, O. S. et al. CO_2 electroreduction to ethylene via hydroxide-mediated copper catalysis at an abrupt interface. *Science* **2018**, *360*, 783–787.

[25] De Luna, P.; Quintero-Bermudez, R.; Dinh, C. T.; Ross, M. B.; Bushuyev, O. S.; Todorović, P.; Regier, T.; Kelley, S. O.; Yang, P. D.; Sargent, E. H. Catalyst electro-redeposition controls morphology and oxidation state for selective carbon dioxide reduction. *Nat. Catal.* **2018**, *1*, 103–110.

[26] Zhuang, T. T.; Liang, Z. Q.; Seifitokaldani, A.; Li, Y.; De Luna, P.; Burdyny, T.; Che, F. L.; Meng, F.; Min, Y. M.; Quintero-Bermudez, R. et al. Steering post-C-C coupling selectivity enables high efficiency electroreduction of carbon dioxide to multi-carbon alcohols. *Nat. Catal.* **2018**, *1*, 421–428.

[27] Zhang, Z.; Xiao, J. P.; Chen, X. J.; Yu, S.; Yu, L.; Si, R.; Wang, Y.; Wang, S. H.; Meng, X. G.; Wang, Y. et al. Reaction mechanisms of well-defined metal-N_4 sites in electrocatalytic CO_2 reduction. *Angew. Chem., Int. Ed.* **2018**, *57*, 16339–16342.

[28] Furuya, N.; Matsui, K. Electroreduction of carbon dioxide on gas-diffusion electrodes modified by metal phthalocyanines. *J. Electroanal. Chem. Interfacial Electrochem.* **1989**, *271*, 181–191.

[29] Zagal, J. H.; Griveau, S.; Silva, J. F.; Nyokong, T.; Bedioui, F. Metallophthalocyanine-based molecular materials as catalysts for electrochemical reactions. *Coord. Chem. Rev.* **2010**, *254*, 2755–2791.

[30] Sorokin, A. B. Phthalocyanine metal complexes in catalysis. *Chem. Rev.* **2013**, *113*, 8152–8191.

[31] Zhang, X.; Wu, Z. S.; Zhang, X.; Li, L. W.; Li, Y. Y.; Xu, H. M.; Li, X. X.; Yu, X. L.; Zhang, Z. S.; Liang, Y. Y. et al. Highly selective and active CO_2 reduction electrocatalysts based on cobalt phthalocyanine/carbon nanotube hybrid structures. *Nat. Commun.* **2017**, *8*, 14675.

[32] Yoshida, T.; Kamato, K.; Tsukamoto, M.; Iida, T.; Schlettwein, D.; Wöhrle, D.; Kaneko, M. Selective electroacatalysis for CO_2 reduction in the aqueous phase using cobalt phthalocyanine/poly-4-vinylpyridine modified electrodes. *J. Electroanal. Chem.* **1995**, *385*, 209–225.

[33] Ju, W.; Bagger, A.; Hao, G. P.; Varela, A. S.; Sinev, I.; Bon, V.; Roldan Cuenya, B.; Kaskel, S.; Rossmeisl, J.; Strasser, P. Understanding activity and selectivity of metal-nitrogen-doped carbon catalysts for electrochemical reduction of CO_2. *Nat. Commun.* **2017**, *8*, 944.